International Journal of Mechanical Sciences 194 (2021) 106206

Contents lists available at ScienceDirect

International Journal of Mechanical Sciences

journal homepage: www.elsevier.com/locate/ijmecsci

Synergistic use of piezoelectric and shape memory alloy elements for vibration-based energy harvesting

Arthur Adeodato[a], Brenno T. Duarte[a], Luciana Loureiro S. Monteiro[a], Pedro Manuel C.L. Pacheco[a], Marcelo A. Savi[b,*]

[a] Centro Federal de Educação Tecnológica Celso Suckow da Fonseca, CEFET/RJ - Department of Mechanical Engineering 20.271.110, Rio de Janeiro, Brazil
[b] Universidade Federal do Rio de Janeiro, COPPE - Department of Mechanical Engineering, Center for Nonlinear Mechanics 21.941.972, Rio de Janeiro, PO Box 68.503, Brazil

ARTICLE INFO

Keywords:
Energy harvesting
Piezoelectric materials
Shape memory alloys
Experimental analysis
Numerical analysis

ABSTRACT

The efforts for clean and renewable energy have been encouraging a growing interest for vibration-based energy harvesting devices. Piezoelectric materials are remarkable elements to promote electro-mechanical coupling allowing the conversion of the mechanical vibration into electrical power through piezoelectric direct effect. Nevertheless, this promising application is associated with the key challenge to enhance and expand the energy harvesting capacity. In this regard, this work proposes the synergistic use of smart materials, combining piezoelectric and shape memory alloy (SMA) elements. Experimental and numerical analyses are performed showing the enhanced capabilities of the system due to the adaptability provided by shape memory alloys. A piezoelectric beam excited by an electrodynamics shaker is connected with a shape memory alloy element that allows to exploit its remarkable characteristics in order to change system properties with temperature variations through Joule's effect. Thermomechanical tests are performed for SMA characterization. Afterward, nonlinear dynamics of the energy harvesting system is investigated exploiting the SMA adaptive behavior. Results show that the synergistic use of smart materials is able to increase the device bandwidth, improving the system performance for energy harvesting purposes.

1. Introduction

Vibration-based energy harvesting has a growing importance nowadays due to the possibility to provide power to portable devices eliminating the need for frequent battery replacements and power cables. Smart materials are essential in this process, promoting the conversion between mechanical and electrical fields. There are several possible alternatives for this aim and piezoelectric materials are the most common one.

A piezoelectric energy harvester can be understood as a mechanical system connected to an electrical system by a piezoelectric element. In general, this electro-mechanical system has an effective conversion when external source frequencies match with harvester natural frequency and, therefore, the harvesting system works under resonant conditions [1–4]. As a consequence, piezoelectric harvesters present a narrow bandwidth. Since the ambient vibrations are usually frequency-varying or random, there is a nowadays challenge to enhance the energy harvesting capacity, and the inclusion of nonlinearities has shown to be a promising approach [5].

The literature presents several investigations that seek the increase the energy harvesting capacity through the incorporation of nonlinear effects: bi-stable structures [6–8], mechanical pre-loads [9], magnetic tip mass [10–12], convenient geometries [13–16], mechanical end-stops [17–20], electrical circuits [21–23], among others. Due to external source fluctuations, random analysis is also relevant, defining proper aspects of operational conditions [11,24].

The seek for proper device configuration is another approach that has been investigated to enhance energy harvesting capacity. In this regard, it is interesting to mention some references that employed analytical, numerical and experimental analyses confirming that nonlinear effects contribute to a substantial enhancement of the energy harvester capacity: M-shaped bent clamped beam [25], nonuniform buckled beam [26], T-shaped element [27] and snap-through buckling mechanism [28].

The synergistic use of smart materials is another interesting, promising approach. The combination of piezoelectric and shape memory alloy (SMA) confers adaptive characteristics to the system. SMA has as essential thermomechanical characteristic the solid-phase transformations induced either by stress or by temperature fields. Typically, SMA

* Corresponding author.
E-mail address: savi@mecanica.ufrj.br (M.A. Savi).

https://doi.org/10.1016/j.ijmecsci.2020.106206
Received 13 August 2020; Received in revised form 3 November 2020; Accepted 14 November 2020
Available online 19 November 2020
0020-7403/© 2020 Elsevier Ltd. All rights reserved.

has two phases, austenite and martensite, with different properties for each one. In addition, phase transformation phenomena are related to hysteretic behavior, which means that it dissipates energy during the transformation cycle. Temperature-induced phase transformations can be exploited on piezoelectric energy harvesters in order to confer adaptability that allows the alteration of system resonant conditions by temperature changes. On the other hand, stress-induced phase transformations exploit the hysteretic characteristics that present high dissipation level.

Avirovik et al. [29] developed a hybrid device coupling piezoelectric and SMA elements for dual functionality, both as actuator and energy harvester. deMarqui et al. [30] developed a finite element analysis for a piezoelectric cantilever beam with a resistance element and base vibration for energy harvesting in air vehicles. deSouza and deMarqui [31] studied the dynamical influence of pseudoelastic helical springs coupled to a two degree of freedom airfoil device subjected to different levels of pre-load. Numerical and experimental results are presented exploiting the martensitic phase transformation for both structural damping and energy harvesting. Eugeni et al. [32] presented numerical and experimental investigations of piezoelectric energy harvester based on flag-flutter. Kaur et al. [33] developed an experimental study on piezoelectric energy harvesting from wind and ambient structural vibrations for wireless structural health monitoring. Silva et al. [34] presented a numerical analysis of an SMA-piezoelectric energy harvesting system where both temperature-induced and stress-induced phase transformations are concerned. Results indicated that the inclusion of the SMA element can be used to extend the operational range of the system.

Shape Memory alloy systems have a complex nonlinear dynamics. Savi [35] presented a general overview of nonlinear dynamics of SMA systems. Property changes and dissipation characteristics of an SMA cantilever beam were studied by Li and Feng [36] with the objective to analyze the influence of these aspects in a frequency response curve and the phenomenon of resonance peak shift. Further, Doare et al. [37] presented results of relative higher levels of strain and observed, experimentally, dynamical jumps for angular displacement measured in frequency response diagrams. de Aguiar et al. [38] presented an experimental investigation of the vibration reduction of SMA dynamical systems. Enemark et al. [39] and Enemark et al. [40] discussed SMA dynamical systems with pseudoelastic helical springs achieving interesting results related to equilibrium points and system dissipation. Saadat et al. [41] presented an overview of seismic applications of NiTi shape memory alloys. Wang et al. [42] and Varela and Saiddi [43] performed an experimental analysis of vibration attenuation devices. Recently, several works are being developing exploiting SMA dynamical behavior for different purposes [44–47].

The design of energy harvesting systems needs to include a proper investigation of fatigue life. Smart materials present both structural and functional fatigue. Shape memory alloy fatigue has been studied by several references [48–50] showing that one of the major relevant aspect to shortening fatigue life is the maximum stress of the loading process. Concerning piezoelectric materials, relevant aspects include temperature and electric fields [51–53], indicating that there is an ideal field amplitude window with large polarization and low fatigue degradation. Furthermore, crack development has been reported as the preponderant form of piezoelectric failure [54].

This paper deals with experimental and numerical investigations of the synergistic use of piezoelectric and shape memory alloy elements in a vibration-based energy harvesting system. An experimental apparatus is built considering a piezoelectric cantilever beam connected with an SMA helical spring, excited by an electrodynamics shaker. This energy harvester has adaptive behavior provided by the SMA element and therefore, mechanical properties are altered due to phase transformations induced by temperature changes through Joule's effect. Numerical simulations are carried out comparing results with experimental data. Situations with small amplitudes are of concern and hence, only temperature-induced phase transformations are treated. Therefore, hysteretic behavior due to stress-induced phase transformations is neglected. This condition is favorable for fatigue life issues, avoiding undesirable functional fatigue effects. It is noticeable that the incorporation of the SMA element can be used to enhance the energy harvesting capacity, increasing the operational frequency range of the system. The main goal of this contribution is a proof of concept and the energy cost to promote temperature change is not treated. In this regard, it should be highlighted that the system design needs to be developed in order to have proper amount of net energy and some available external energy source can be used to provide the necessary energy.

Table 1
SMA helical spring: geometrical and mechanical properties.

Mean ϕ (mm)	wire ϕ (mm)	Spires	Initial Length (mm)
5.6	0.8	20	25

2. Experimental approach and methodology

This section describes a vibration-based energy harvesting experimental approach that employs a synergistic use of piezoelectric and shape memory alloy elements. Themomechanical properties of the SMA element is evaluated through characterization tests. Methodology analysis is also of concern.

2.1. Experimental apparatus

A piezoelectric element (PZT 5H - 40×10×0.5 mm - Mid Technology) is bonded to an aluminum cantilever beam with dimensions: 275×30×2 mm. The cantilever beam is clamped to an electrodynamics shaker (V350-DataPhysics Signal Force) that provides vibration to the system. A shape memory helical spring with a mean diameter of 5.6 mm, wire diameter of 0.8 mm and length of 25 mm (Dynalloy 3-642 NiTi spring tension model) is attached to the free end of the aluminum cantilever beam with the other end fixed to a rigid support. It is considered that martensitic phase is stable at low temperatures, while austenite is stable at high temperatures. It is employed an SMA helical spring that presents martensitic phase at room temperature. Temperature changes are induced through Joule effect by the application of electric current using a stabilized current source (TOE 8950). The geometrical properties of the SMA helical spring is presented in Table 1. The energy harvesting electric circuit is represented by a simple external electric load resistance of 150 kΩ. A picture of the experimental setup is shown by Fig. 1.

A laser displacement transducer (Micro-Epsilon $\mu\epsilon$ model optonNCDT2200) is employed to measure the free end displacement while the base acceleration is evaluated by an accelerometer (PCB 333B40) connected to the shaker. A load cell Leader CS-5 is employed to measure the restitution force provided by the SMA spring. A data acquisition system (CDAQ-9174 National Instruments) is employed. The system is subjected to a harmonic excitation with maximum value of $9.81\ m/s^2$.

Energy harvesting capacity is evaluated by estimating the output and input powers. Output power is calculated by the square of electrical voltage measured in piezoelectric element divided by the external electric resistance element. On the other hand, input power is estimated as the product of the applied force by the velocity measured at the cantilevered beam end connected to the SMA spring. Efficiency is estimated as the ratio between output and input powers.

2.2. Thermomechanical characterization

The thermomechanical characterization of the SMA helical spring starts considering Differential Scanning Calorimeter - DSC (Netzsch DSC 200 F3) tests in order to identify the phase transformation temperatures.

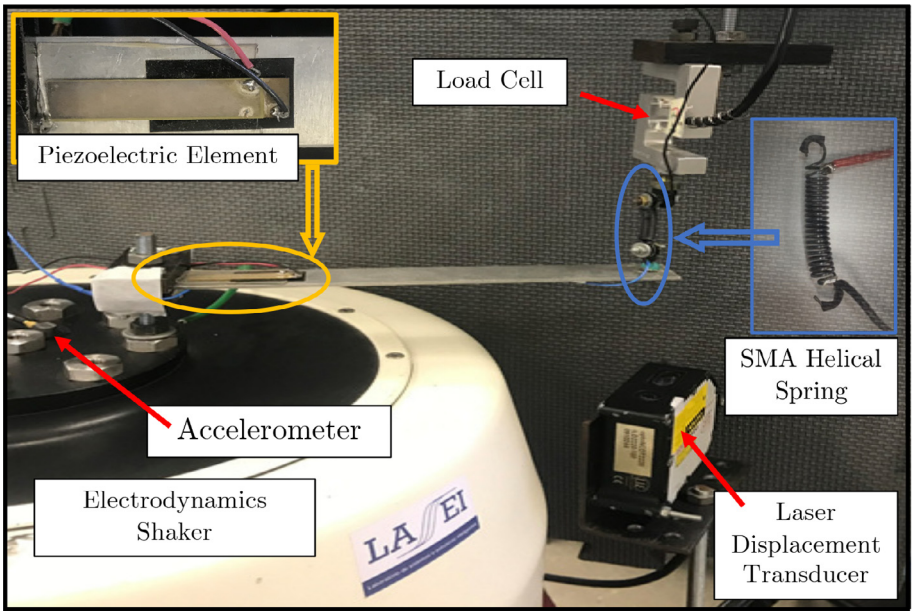

Fig. 1. Experimental apparatus of the energy harvester with synergistic use of piezoelectric and shape memory alloy elements. The system is composed by a cantilever beam with piezoelectric element connected to a shape memory alloy spring, being excited in vertical direction by an electrodynamics shaker.

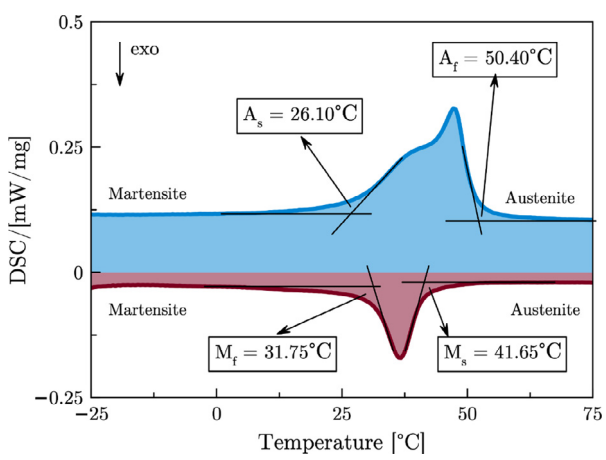

Fig. 2. Differential Scanning Calorimetry analysis showing phase transformation temperatures of an SMA helical spring sample.

Table 2
Phase transformation temperatures from Differential Scanning Calorimetry test.

M_s(°C)	M_f(°C)	A_s(°C)	A_f(°C)
41.65	31.75	26.10	50.40

DSC analysis considers a small SMA sample that is compared with a reference sample. In this test, the energy necessary to follow a prescribed temperature history of the sample is monitored. During phase transformation, latent heat contributes to the sample temperature change and there is a energy variation without temperature change. Fig. 2 presents results of the DSC test for the increase and decrease temperature stages, respectively allowing the estimation of martensite-austenite and austenite-martensite phase transformations. Table 2 summarizes the mean values of phase transformation temperatures. It should be pointed out that ambient temperature is associated with the martensitic phase.

Since temperature is induced by Joule effect, the relation between electric current and temperature can be estimated by considering a contactless infrared sensor (MLX90614 GY-906) that uses an Arduino Uno board for data acquisition. SMA spring is connected with two fixed terminals to which a current from 0.0 A to 2.5 A is applied with an increment of 0.1 A and interval of 60 s between each increment. This allows one to build a temperature-electrical current curve, presented in Fig. 3, where the phase transformation temperatures obtained from DSC analysis are represented.

The SMA spring is now characterized by a quasi-static mechanical tensile test. Force-displacement curves are built by using an Instron testing system (5966 model) with a controlled displacement rate of 10 mm/min. Tests are carried out for different, constant electric currents (0 A and 1.5 A). Fig. 4 presents force-displacement curves for the quasi-static tests, showing shape memory effect behavior for low temperature (0 A) and pseudoelastic effect for high temperature behavior (1.5 A). Stiffness can be estimated by considering the slope of the linear part of the curve, following the procedure presented by Savi et al. [55]. The slope is calculated considering points selected in the region from 30% to 70% of the maximum load for martensite (0.0 A). Analogously, considering points from 10% to 40% of the maximum load for austenite (1.5 A). This methodology reduces the influence of instability effects related to experimental measurements at the beginning of the test and at the load reversal regions. This analysis indicates $k_M = 216$ N/m for detwined maternsite and $k_A = 288$ N/m for austenitic phase. Note that, the application of electric current causes the increase of the critical stress level where phase transformation begins to occur.

3. Mathematical model

This section is dedicated to establish a mathematical model to describe the energy harvesting system based on the experimental apparatus of the preceding section. In essence, this system is a mechanical oscillator connected to an electric system by the piezoelectric element. Fig. 5 presents the experimental apparatus sketch and the equivalent electro-mechanical system.

The dynamical system can be described by two coupled differential equations representing the mechanical and the electrical systems [1,11,56,57].

$$m\ddot{z} + c\dot{z} + k_{beam}z + F_{SMA} - \theta V = -m\ddot{y} \tag{1}$$

$$\theta\dot{z} + C_p\dot{V} + \frac{V}{R} = 0 \tag{2}$$

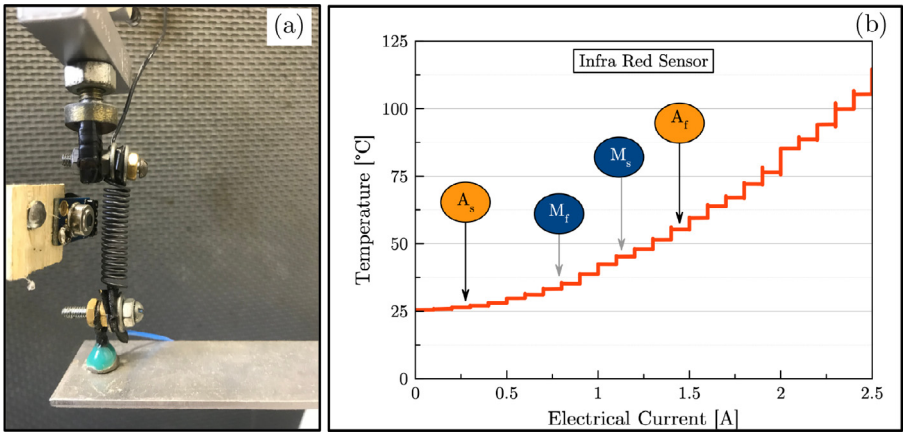

Fig. 3. Experimental analysis of the temperature-electrical current. (a) Experimental apparatus of the SMA helical spring for the measurement through infra red sensor. (b) Temperature-electrical current diagram.

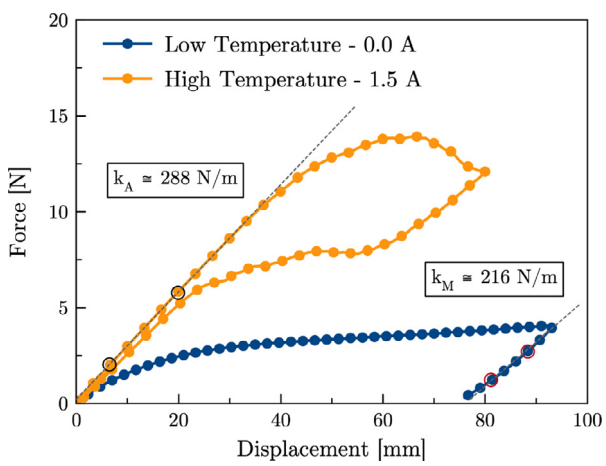

Fig. 4. Quasi static force-displacement curves of the SMA helical spring considering different electrical currents. Ambient (low) temperature - without electrical current (0 A); and high temperature - with 1.5 A.

where z is the relative displacement between x - body displacement related to a inertial referential, and y - base displacement: $z = x - y$; m is the equivalent mass, c is the total dissipation coefficient and k_{beam} represents the beam stiffness; the eletro-mechanical coupling provided by the piezoelectric element is represented by θ while C_p and R are circuit capacitance and resistance, respectively; $\ddot{y} = A_0 \cos(\omega t)$ where A_0 is the maximum acceleration base-vibration amplitude, and F_{SMA} is the restitution force provided by the shape memory alloy element. Eqs. (1) and (2) are solved trough the fourth-order Runge-Kutta method implemented in a C programming language code. All simulation tests are performed considering null initial conditions for displacement, velocity and electrical tension.

The beam characterization is based on *Euller-Bernoulli* assumptions allowing the estimation of an equivalent stiffness of the cantilevered beam. Therefore, the bending moment ($M(s)$) across the cantilever beam can be expressed by the second derivative of beam deflection ($w(s)$) times the bending coefficient (EI) as following:

$$EI\frac{\partial^2 w}{\partial s^2} = M(s) \tag{3}$$

where s is a coordinate oriented from the clamp to the free end and varies from zero to L. E represents the elastic modulus (70 GPa for aluminum), I is the cross section moment of inertia ($\frac{bh^3}{12}$) and L is the beam length. By considering a cantilever beam ($w(0) = 0$ and $w'(0) = 0$), it is possible to define the following stiffness:

$$k_{beam} = \frac{3EI}{L^3} = 213 \quad N/m \tag{4}$$

Since an SMA helical spring is connected to the end of the beam, the equivalent stiffness of the mechanical system can be calculated by the following expression

$$k_{eq} = k_{beam} + k_{SMA} \tag{5}$$

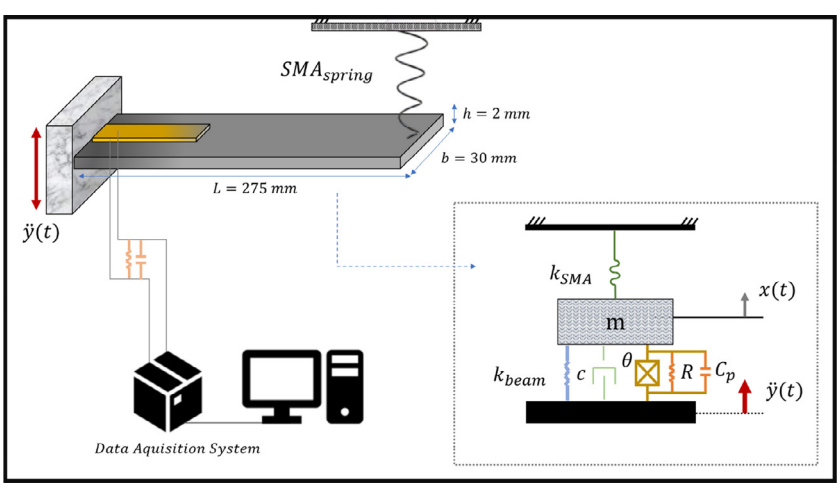

Fig. 5. Dynamical model of the energy harvester with synergistic use of piezoelectric and shape memory alloy elements. Cantilever piezoelectric beam coupled to SMA helical spring and its representation as a single degree of freedom oscillator.

where it is important to observe that, actually, k_{SMA} has two possible values, depending on the phase (martensite or austenite), which is defined by the temperature.

The estimation of the equivalent mass has been treated by many authors [1,6,57]. Literature refers to models that considers a distributed mass along the beam and also a concentrated mass (tip mass) at the free end. In order to establish the equivalent mass, consider the kinetic energy of the beam and integrating a shape function. Considering the maximum beam kinetic energy:

$$T_{\max} = \frac{1}{2}\int_0^L \frac{m}{L}\dot{w}(s)^2 dx \tag{6}$$

By considering the beam theory to express the velocity variation $\dot{w}(s)$, it is written:

$$\dot{w}(s) = \frac{\dot{w}_{\max}}{2L^3}(3s^2L - s^3) \tag{7}$$

consequently, Eq. (6) becomes:

$$T_{\max} = \frac{1}{2L}\left(\frac{\dot{w}_{\max}}{2L^3}\right)^2 \int_0^L (3s^2L - s^3)^2 dx = \frac{1}{2}\left(\frac{33}{140}m\right)\dot{w}_{\max}^2 \tag{8}$$

If m_{eq} represents the equivalent mass for a cantilever beam reduced to a single degree of freedom, the maximum kinetics energy can be expressed as:

$$T_{\max} = \frac{1}{2}m_{eq}\dot{w}_{\max}^2 \tag{9}$$

combining Eqs. (8) and (9), considering aluminum's density ($\rho_{Al} = 2700 kg/m^3$) and the beam dimensions, the equivalent mass is as follows,

$$m_{eq} = \frac{33}{140}\rho\Lambda + M_t = 10 \ \ g \tag{10}$$

where M_t represents the tip mass added on the free end of a cantilever beam. Here, no expressive tip mass is used in the experimental apparatus and therefore, it is neglected. Hence, the equivalent mass of the mechanical system is the product of the material density (ρ) and its volume (Λ), times 33/140 coefficient.

For the considered situations, the helical spring is subjected to stress levels that are below critical stresses, which means that stress-induced phase transformations are neglected. Therefore, only temperature-induced phase transformation is of concern and the SMA helical spring presents a linear response, but with different stiffness: martensitic low temperature behavior and austenitic high temperature behavior.

Based on that, k_{eq} assumes two different values: $k_{eq}^M = 429 N/m$ for martensitic phase; and $k_{eq}^A = 501 N/m$ for austenite. Under these assumptions, the single degree of freedom equivalent mechanical system has two possible natural frequency: $\omega_n^M = 32.96 \ \ Hz$ and $\omega_n^A = 35.61 \ \ Hz$. Therefore, it is expected a variation of resonance frequency peaks around 2.65 Hz (35.61–32.96) which means 8.04% of variation with respect to low temperature resonance frequency value.

Based on the same assumptions, the shape memory alloy helical spring force can be expressed by

$$F_{SMA} = k_{SMA} z \tag{11}$$

where k_{SMA} alternates from martensitic to austenite characteristics when temperature changes from low to high temperature behaviors, according to the values presented in Fig. 4.

Concerning the Joule effect, experimental tests presented in Fig. 3 are employed in order to define a temperature-electric current relation as follows,

$$T(i) = 12.78i^2 + 1.14i + 25 \tag{12}$$

where i is the electrical current. Besides, phase transformation temperatures are assumed to be defined based on the DSC temperatures. For the sake of simplicity, it is defined T_M as the temperature below which only martensitic phase is stable, being considered in such a way that $T_M \leq M_f$. Since $A_s < M_f$ it is also assumed that $T_M < A_s$. Therefore, it is adopted $T_M = 25°C$, assumed to be the ambient temperature. The temperature above which only austenite is stable in a stress-free state, needs to be $T_A \geq A_f$, being defined as $T_A = A_f = 50.4°C$. In terms of electric current, it is considered that the helical spring is in the martensitic state for 0 A, while a austenitic state is related to values greater than 1.37 A.

Table 3
Parameters of the 1 degree of freedom piezoelectric-shape memory alloy energy harvester.

$m_{eq}(kg)$	$k_{beam}(N/m)$	$\theta(N/V)$	$C_p(F)$	$R(Ohm)$	$A_0(m/s^2)$
0.01	213	-3.1×10^{-5}	2.48×10^{-8}	150×10^3	9.81

Table 4
Shape memory alloy parameters for low and high temperatures.

$T_M(°C)$	$T_A(°C)$	$c_M(Ns/m)$	$c_A(Ns/m)$	$k_M(N/m)$	$k_A(N/m)$
25	50.4	0.05	0.0335	216	288

Damping coefficient associated with martensitic, c_M, and austenitic, c_A, phases are estimated in order to match experimental results. The same procedure is employed for the electro-mechanical coupling, θ. Capacitance is defined in terms of constrained permittivity: $C_p = \frac{A_p \epsilon_{33}}{t_p}$ according to Kim et al. [3], where A_p and t_p are piezoelectric element surface area and thickness, respectively; ϵ_{33} is considered as the product of piezo dielectric constant (3500, provided in data sheet) and the vacuum permittivity (8.85×10^{-12} F/m). Tables 3 and 4 show parameters employed for numerical simulations.

The energy harvesting performance is monitored by considering input power P_{in} that is essentially the mechanical power; and the output power P_{out}, which is associated with the electrical power.

$$P_{in} = m\ddot{y}\dot{z} = m_{eq}A_0 cos(\omega t)\dot{z} \tag{13}$$

$$P_{out} = \frac{V^2}{R} \tag{14}$$

System efficiency can be evaluated by considering the ratio between output and input power.

$$\eta = \frac{P_{out}}{P_{in}} \tag{15}$$

Since the system responses are essentially linear for each phase, it is possible to obtain analytical expressions for displacement and output power, employed for numerical simulation verification [6,56]. Based on that, it is possible to define an expression for relative displacement, z^a, as a function of input acceleration $\ddot{y}$

$$z^a = \ddot{y}\frac{\omega_N^{-2}\sqrt{1+(r\Omega)^2}}{\sqrt{(1-(1+2r\zeta)\Omega^2)^2 + ((1+\kappa^2)r\Omega + 2\zeta\Omega - r\Omega^3)^2}} \tag{16}$$

Concerning the output power, p_{out}^a, and the input power, p_{in}^a, the following expressions are written:

$$p_{out}^a = \ddot{y}^2\frac{m_{eq}(\omega_N^{-1})r\kappa^2\Omega^2}{(1-(1+2r\zeta)\Omega^2)^2 + ((1+\kappa^2)r\Omega + 2\zeta\Omega - r\Omega^3)^2} \tag{17}$$

$$p_{in}^a = m_{eq}\dot{z}^a\ddot{y} \tag{18}$$

These definitions allow one to present an analytical expression for the system efficiency η^a,

$$\eta^a = \frac{p_{out}^a}{p_{in}^a} \tag{19}$$

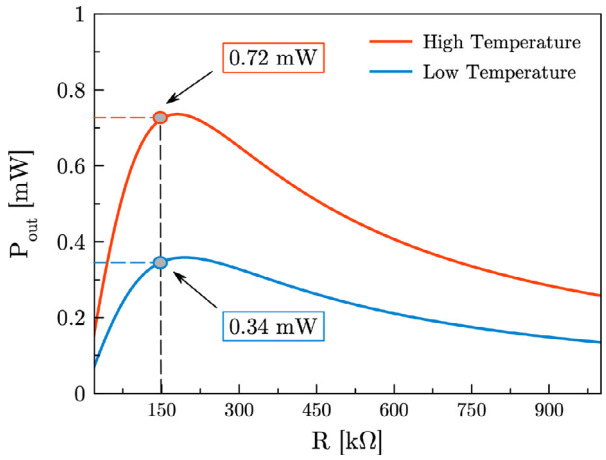

Fig. 6. Analysis of the energy harvester maximum output power as a function of external resistance load for low and high SMA temperature conditions.

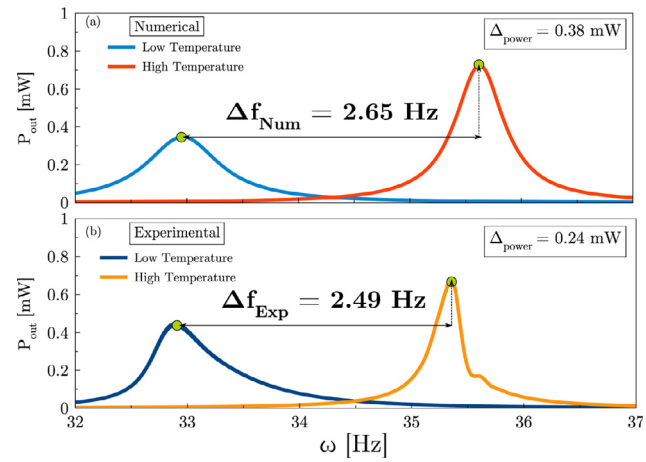

Fig. 8. Energy harvester bandwidth analysis highlighting the adaptive capacity provided by shape memory alloys, increasing of the output power. (a) Numerical simulations. (b) Experimental data.

where $r = (\omega_N RC_p)$, $\kappa^2 = \theta^2/(k_{eq}C_p)$, $\Omega = \omega/\omega_n$ is the ratio between base vibration frequency and system natural frequency and $\zeta = c/(2m_{eq}\omega_n)$.

4. Results and discussion

Numerical simulations are performed employing the fourth-order Runge-Kutta method. Parameters presented in the previous sections are employed for all simulations and compared with experimental data. Convergence analysis is performed defining a time step $dt = \tau/200$, where τ represents the forcing frequency period.

Initially, a diagram is built with an up-sweep test evaluating the maximal power obtained as a function of electrical resistance. Fig. 6 shows this diagram for two different temperatures: low temperature, where

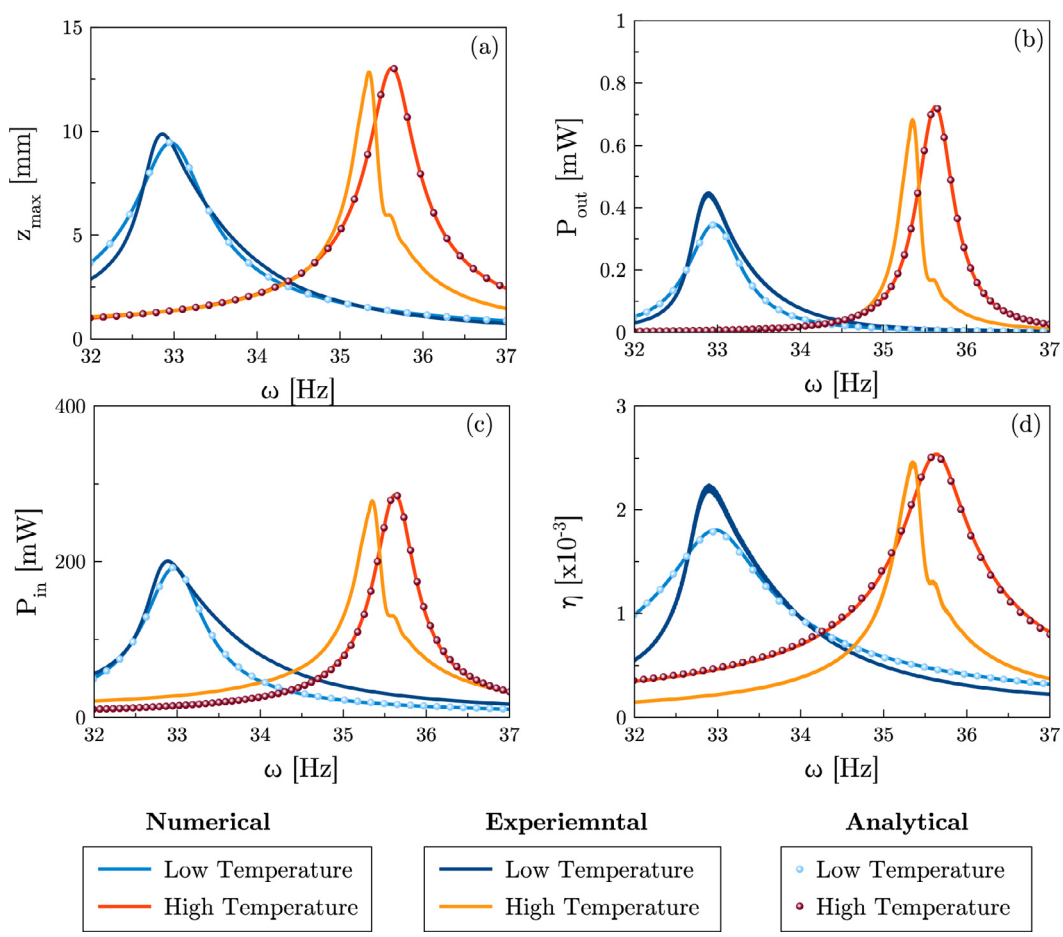

Fig. 7. Experimental, analytical and numerical results of the energy harvester frequency response. System adaptability is represented by the temperature dependent resonant conditions. (a) Maximum Displacement. (b) Maximum Output Power. (c) Maximum Input Power. (d) Maximum Efficiency.

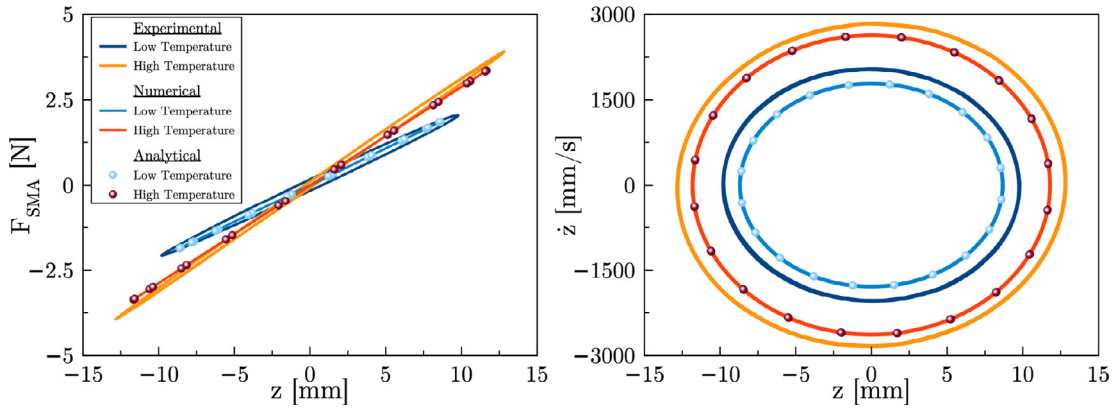

Fig. 9. Energy harvester steady state response comparing low and high temperature resonant stationary conditions. (a) Force-displacement curve. (b) Phase space.

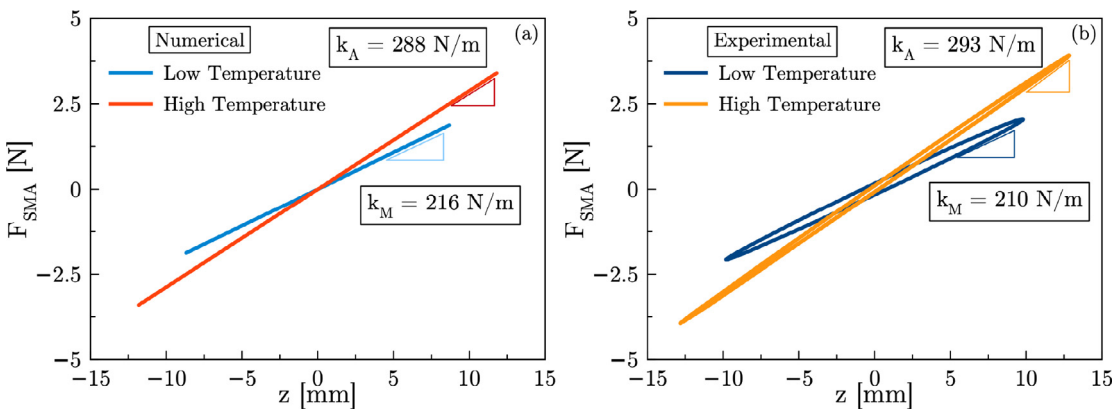

Fig. 10. Energy harvester force-displacement curves comparing low and high temperature resonant stationary conditions. (a) Numerical simulations. (b) Experimental data.

martensitic phase is stable; and high temperature, where austenite is stable. Based on these results, it is possible to identify load resistance associated with the maximum output power values for both temperatures, representing the optimal operational conditions for energy harvesting purposes. It is noticeable that the optimal resistances are 190 kΩ for low temperature with a maximum output power of 0.35 mW. For high temperature, an optimal resistance of 180 kΩ is identified, being associated with an output power of 0.73 mW. Despite these values, the experimental apparatus considers an electrical resistance of 150 kΩ. For this reason, 150 kΩ is adopted for numerical simulations and it is expected a maximum value of 0.34 and 0.72 mW for each case, respectively.

Frequency response diagrams are now of concern, varying frequency in a forward direction with a value of maximum acceleration amplitude equal to 9.81 m/s^2, and capturing the maximum value of each variable - displacement, output power, input power and efficiency. Numerical simulations considers one hundred cycles for each value of frequency. Two different temperatures are treated, considering two currents: 0 A and 2.5 A. Numerical simulations and analytical analyses are compared with experimental data, showing a good agreement (Fig. 7). It is noticeable that the system presents two resonant conditions, one for each temperature, showing the adaptability conferred by the SMA. Experimental results presented a 2.49 Hz (35.35–32.86) range between maximum peaks representing a variation of 7.5% with respect to the resonance frequency related to low temperature.

Fig. 8 shows a different perspective of the adaptive behavior of the energy harvester, highlighting the peaks where maximum output power occurs. Also, system bandwidth is measured from peak to peak. In this regard, Δf becomes the difference between frequency peaks and Δ_{power} the increase of the output power.

In summary, it is clear that the adaptive behavior can change resonant conditions for two different levels, considering different temperatures or electric current applied. Therefore, the combination of piezoelectric and SMA defines a two-peak resonant system that can be adjusted based on the excitation conditions. This allows a broad bandwidth system and this behavior helps to enhance energy harvesting capacity. Numerical-analytical and experimental results are in close agreement and the discrepancies can be related to thermal variations, fixation conditions and geometric parameters.

In order to evaluate the different behaviors related to each resonant condition, steady state responses are now of concern (Fig. 9). The idea is to evaluate the low and high temperature resonant conditions. Fig. 9(a) presents force-displacement curves and (b) phase spaces for each temperature, showing the stiffness changes and the different amplitudes for each case. Note that numerical, analytical and experimental approaches are presented, showing good agreements. Numerical maximum displacements varies 3.11 mm (from 8.68 to 11.81 mm) while experimental maximum displacements present a variation of 3.04 mm (from 9.8 to 12.84 mm). It means an increase of 26.5% for numerical case while 23.6% for experimental.

Fig. 10 shows details of the force-displacement curve employed to assess the stiffness variation of the SMA helical spring for low and high temperature conditions. Numerical simulations, Fig. 10(a), show only stiffness change since the SMA element behaves in linear elastic regime of martensite (low temperature) and austenite (high temperature). Experimentally, Fig. 10(b), it is observed small hysteresis responsible to an additional dissipation with the temperature increase. This hysteretic behavior alters the dissipation and consequently, the maximum amplitude of the system response.

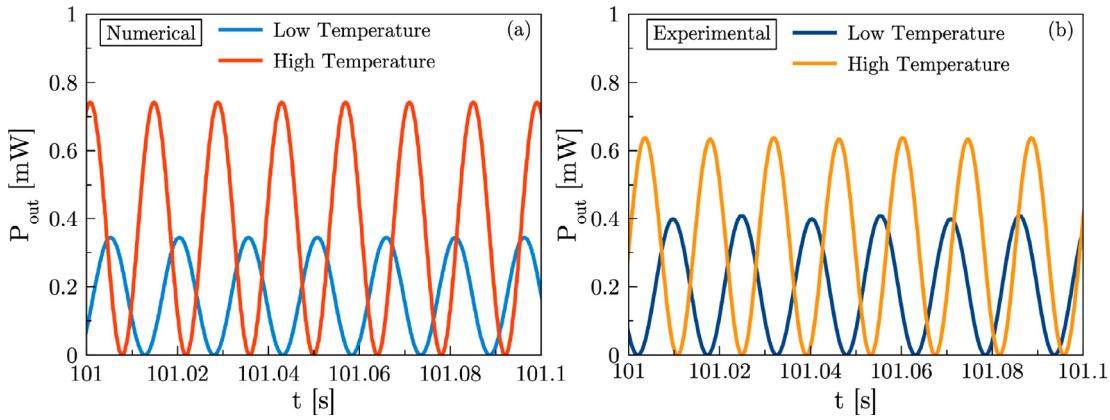

Fig. 11. Energy harvester output power time history for a fixed forcing frequency comparing low and high temperature responses. (a) Numerical output power (ω = 32.96 Hz for low temperature and ω = 35.61 Hz for high temperature). (b) Experimental output power (ω = 32.86 Hz for low temperature and ω = 35.35 Hz for high temperature).

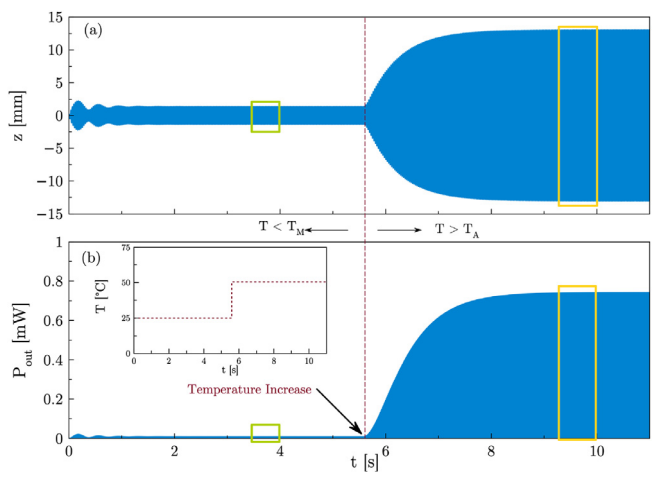

Fig. 12. Time evolution of the energy harvester response considering the temperature increase and a forcing frequency of 35.61 Hz. (a) Displacement. (b) Output Power.

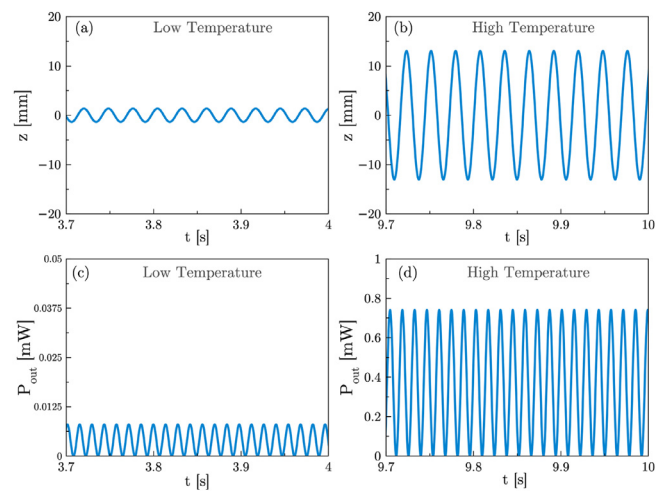

Fig. 13. Details about the energy harvester steady state responses for ω = 35.61 Hz and different temperatures. (a) Low temperature displacement - $T < T_M$. (b) High temperature displacement - $T > T_A$. (c) Low temperature output power - $T < T_M$. (d) High temperature output power - $T > T_A$.

Fig. 11 shows steady state time history of the output power for each specific resonance stationary excitation frequency. Fig. 11(a) presents numerical results while Fig. 11(b) presents experimental results. Both cases have the output power trend with maximum values that are in agreement with the values expected from Figs. 6 and 8.

The adaptive characteristic of the energy harvesting system is now of concern showing an emblematic numerical simulation associated with the synergistic use of smart materials. Consider a situation where the forcing frequency is 35.61 Hz at room temperature, where the system is at martensitic phase. Under this condition, the system presents a small amplitude response, associated with a low output power. In order to alter this condition, the temperature is increased by applying an electric current of 1.37 A, which promotes a phase transformation from martensite to austenite, causing the SMA stiffness change. Under the new condition, the excitation frequency matches system high temperature natural frequency, promoting higher levels of amplitude and, consequently, higher levels of converted output power. Fig. 12 presents numerical simulations of this case while Fig. 13 presents details about the steady state system response for each one of the regions presented. This change represents an increase from 1.34 to 13.02 mm (around 10 times) on system maximum amplitude and from 0.008 to 0.72 mW (around 100 times) on the maximum output power. It should be pointed out that this test is a proof of concept simulation where the energy cost is not of concern. A proper system design should be analyzed in order to evaluate the net energy but, it is possible to imagine the use of some available external source to provide the necessary energy.

5. Conclusions

This paper presents experimental and numerical investigations of the synergistic use of smart materials - piezoelectric and shape memory alloy - for vibration-based energy harvesting purposes. The harvester configuration is composed by a piezoelectric cantilever beam connected to an SMA spring and excited by an electrodynamics shaker that represents the energy source. SMA provides an adaptive characteristic due to solid-phase transformations.

The SMA element presents martensitic phase at room temperature and austenitic phase at high temperature. Therefore, temperature changes promote phase transformations associated with property alterations. The temperature change is induced by the application of electric currents and temperature control provides system adaptability. The system is characterized by two main conditions: martensitic low temperature behavior; and austenitic high temperature behavior. Based on that, energy harvester has an adaptive frequency tuning that is temperature dependent.

Energy harvesting capacity is monitored by displacement, output power, input power and efficiency. The different behaviors related to each resonant condition are analyzed considering force-displacement curves and phase spaces for each temperature, showing the stiffness and dissipation changes together with different amplitudes for each case.

Results show that numerical and experimental results are in close agreement. Temperature changes cause a shift of the system resonance frequency close to 10% that can be exploited for energy harvesting purposes. An improvement of the harvester performance in frequency response is around 0.3 mW (0.38 mW for numerical simulations and 0.24 mW for experimental case) due to temperature increase of the SMA element. Adaptive behavior is highlighted from a stationary forcing frequency case where the temperature increase is able to promote phase transformation and, as a consequence, frequency matches the system high temperature natural frequency. This situation shows an increase of 0.71 mW (around 100 times) at maximum output power and 11.68 mm (around 10 times) for maximum displacement. In this regard, SMA provides a useful adaptive frequency tuning that can be desirable to deal with external source fluctuations. This general idea can extend the operational range of energy harvesting systems, increasing the frequency broadband. The synergistic use of piezoelectric materials and shape memory alloys is able to improve device bandwidth and system performance, promoting an energy harvesting enhancement.

The proposed methodology is a proof of concept and the energy cost to promote temperature change is not of concern. A proper system design needs to be considered in order to evaluate the required energy to promote the SMA temperature change in such a way that an interesting amount of net energy is generated. Nevertheless, situations where a high energy is demanded to promote phase transformations, it is possible to use some external available energy source to provide the needed power. Heat sources are potential interesting candidates for this aim.

Declaration of Competing Interest

The authors declare that they have no conflict of interest.

CRediT authorship contribution statement

Arthur Adeodato: Conceptualization, Methodology, Software, Validation, Formal analysis, Investigation, Writing - original draft. **Brenno T. Duarte:** Conceptualization, Methodology, Software, Validation, Formal analysis, Investigation. **Luciana Loureiro S. Monteiro:** Conceptualization, Methodology, Software, Validation, Formal analysis, Investigation, Supervision, Writing - original draft. **Pedro Manuel C.L. Pacheco:** Conceptualization, Methodology, Software, Validation, Formal analysis, Investigation, Writing - original draft, Supervision, Writing - review & editing. **Marcelo A. Savi:** Conceptualization, Methodology, Software, Validation, Formal analysis, Investigation, Writing - original draft, Supervision, Writing - review & editing.

Acknowledgements

The authors would like to acknowledge the support of the Brazilian Research Agencies CNPq, FAPERJ and CAPES (Grant PROEX 803/2018).

References

[1] Dutoit NE, Wardle BL, Kim S-G. Design considerations for mems-scale piezoelectric mechanical vibration energy harvesters. Integr Ferroelectr 2005;71(1):121–60. doi:10.1080/10584580590964574.
[2] Erturk A, Inman DJ. An experimentally validated bimorph cantilever model for piezoelectric energy harvesting from base excitations. Smart Mater Struct 2009;18. doi:10.1088/0964-1726/18/2/025009.
[3] Kim M, Hoegen M, Dugundji J, Wardle BL. Modeling and experimental verification of proof mass effects on vibration energy harvester performance. Smart Mater Struct 2010;91. doi:10.1088/0964-1726/19/4/045023.
[4] Karadag CV, Topaloglu N. A self-sufficient and frequency tunable piezoelectric vibration energy harvester. J Vibr Acoust 2017;139. doi:10.1115/1.4034775.
[5] Tran N, Ghayesh MH, Arjomandi M. Ambient vibration energy harvesters: a review on nonlinear techniques for performance enhancement. International Journal of Engineering Science 2018;127. doi:10.1016/j.ijengsci.2018.02.003.
[6] Erturk A, Inman DJ. Piezoelectric Energy Harvesting. John Wiley/Sons, Inc; 2011.
[7] Liu H, Zhong J, Lee C, Lee S-W, Lin L. A comprehensive review on piezoelectric energy harvesting technology: materials, mechanisms, and applications. Appl Phys Rev 2018;5. doi:10.1063/1.5074184.
[8] Maaer B, Boughamoura A, El-Bab AMRF, Francis LA, Tounsi F. A review on design improvements and techniques for mechanical energy harvesting using piezoelectric and electromagnetic schemes. Energy Convers Manage 2019;199. doi:10.1016/j.enconman.2019.111973.
[9] Leland ES, Wright PK. Resonance tuning of piezoelectric vibration energy scavenging generators using compressive axial preload. Smart Mater Struct 1985;15. doi:10.1088/0964-1726/15/5/030.
[10] Yang J, Yue X, Wen Y, Li P, Yu Q, Bai X. Design and analysis of a 2D broadband vibration energy harvester for wireless sensors. Sensors and Actuators A: Physical 2014;205 doi:10.1016/j.sna.2013.10.005.
[11] dePaula AS, Inman DJ, Savi MA. Energy harvesting in a nonlinear piezomagnetoelastic beam subjected to random excitation. Mechanical Systems and Signal Processing 2015;54. doi:10.1016/j.ymssp.2014.08.020.
[12] Dhote S, Yang Z, Behdinan K, J Z. Enhanced broadband multi-mode compliant orthoplanar spring piezoelectric vibration energy harvester using magnetic force. International Journal of Mechanical Sciences 2018;135. doi:10.1016/j.ijmecsci.2017.11.012.
[13] Friswell MI, Ali SF, Bilgen O, Adhikari S. Non-linear piezoelectric vibration energy harvesting from a vertical cantilever beam with tip mass. J Intell Mater SystStruct 2012;23. doi:10.1177/1045389X12455722.
[14] Zhou Z, Hobeck JD, Cao J, Inman DJ. Analytical and experimental investigation of flexible longitudinal zigzag structures for enhanced multi-directional energy harvesting. Smart Mater Struct 2017;26. doi:10.1088/1361-665x/26/3/035008.
[15] Leem AJ, Moosavian A, Inman DJ. A piezoelectrically generated bistable laminate for morphing. Materials Letters 2017;190. doi:10.1016/j.matlet.2017.01.005.
[16] Lee AJ, Inman DJ. A multifunctional bistable laminate:snap-through morphing enabled by broadband energy harvesting. J Intell Mater SystStruct 2018;29. doi:10.1177/1045389X18770895.
[17] Basset P, Galayko D, Cottone F, Guillemet R, Blokhina E, Marty F, et al. Electrostatic vibration energy harvester with combined effect of electrical nonlinearities and mechanical impact. J Micromech Microeng 2014;24. doi:10.1088/0960-1317/24/3/035001.
[18] Wu Y, Badel A, Formosa F, Liu W, Agbossou A. Nonlinear vibration energy harvesting device integrating mechanical stoppers used as synchronous mechanical switches. J Intell Mater SystStruct 2014;25. doi:10.1088/1361-665x/26/3/035008.
[19] Woo MS, Ahn JH, Eom JH, Hwang WS, Kim JH, Yanf CH, Song GJ, Hong SD, Jhun JP, Sung TH. Study on increasing output current of piezoelectric energy harvester by fabrication of multilayer thick film. Sensors and Actuators A: Physical 2018;269. doi:10.1016/j.sna.2017.12.025.
[20] Zhang J, Qin L. A tunable frequency up-conversion wideband piezoelectric vibration energy harvester for low-frequency variable environment using a novel impact- and rope-driven hybrid mechanism. Applied Energy 2019;240. doi:10.1016/j.apenergy.2019.01.261.
[21] Wang W, Cao J, Zhang N, Lin J, Liao W. Magnetic-spring based energy harvesting from human motions: design, modeling and experiments. Energy Conversion and Management 2017;132. doi:10.1016/j.enconman.2016.11.026.
[22] Silva TMP, Clementino MA, de Marqui C, Erturk A. Effects of a piezoelectric based nonlinear energy sink on the behavior of an electromechanically coupled beam. Active and passive smart structures and integrated systems XII; 2018. doi:101117/122302682.
[23] Sugino C, Ruzzene M, Erturk A. Design and analysis of piezoelectric metamaterial beams with synthetic impedance shunt circuits. IEEE/ASME Transactions on Mechatronics 2018;23. URL https://ieeexplore.ieee.org/abstract/document/8425786?casa_token=emz_BdzQpnYAAAAA:ughbVEz0f5T-OG1vpiMKUfxS4N1oIXKlErJ0xnn8BIIOn84j1q7a18TPgZ1x_FAxwD3CLhnu9w.
[24] Pereira TL, dePaula AS, Fabro AT, Savi MA. Random effects in a nonlinear vibration-based piezoelectric energy harvesting system. Int J Bifurcation Chaos 2019;29(04):1950046. doi:10.1142/S0218127419500469.
[25] Leadenham S, Erturk A. M-shaped asymmetric nonlinear oscillator for broadband vibration energy harvesting: Harmonic balance analysis and experimental validation. Journal of Soundand Vibration 2014;333(23):6209–23. doi:10.1016/j.jsv.2014.06.046.
[26] Van BL. Nonuniform buckled beam energy harvesting: experimental validation, modeling, and dynamic analysis. UC Santa Barbara; 2016. Phd.
[27] Xie Z, Wang T, Kwuimy CAK, Shao Y, Huang W. Design, analysis and experimental study of a t-shaped piezoelectric energy harvester with internal resonance. Smart Mater Struct 2019;28(8):085027. doi:10.1088/1361-665x/ab2e15.
[28] Speciale A, Ardito R, Baù M, Ferrari M, Ferrari V, Frangi AA. Snap-through buckling mechanism for frequency-up conversion in piezoelectric energy harvesting. Applied Sciences 2020;10(10):3614. doi:10.3390/app10103614.
[29] Avirovik D, Kumar A, Bodnar RJ, Priya S. Remote light energy harvesting and actuation using shape memory alloy-piezoelectric hybrid transducer. Smart Mater Struct 2013;22. doi:10.1088/0964-1726/22/5/052001.
[30] deMarqui C, Erturk A, Inman DJ. An electromechanical finite element model for piezoelectric energy harvester plates. Journal of Soundand Vibration 2009;327. doi:10.1016/j.jsv.2009.05.015.
[31] deSouza CV, deMarqui C. Airfoil-based piezoelectric energy harvesting by exploiting the pseudoelastic hysteresis of shape memory alloy springs. J Intell Mater SystStruct 2015;24. doi:10.1088/0964-1726/24/12/125014.

[32] Eugeni M, Elahi H, Fune F, Lampani L, Mastroddi F, Romano GP, Gaudenzi P. Numerical and experimental investigation of piezoelectric energy harvester based on flag-flutter. Aerospace Science and Technology 2020;97:105634. doi:10.1016/j.ast.2019.105634.
[33] Kaur N, Mahesh D, Singamsetty S. An experimental study on piezoelectric energy harvesting from wind and ambient structural vibrations for wireless structural health monitoring. Adv Struct Eng 2020;23(5):1010–23. doi:10.1177/1369433219886956.
[34] Silva LL, Oliveira SA, Pacheco PMCL, Savi MA. Synergistic use of smart materials for vibration-based energy harvesting. TheEuropean Physical Journal Special Topics 2015;224. doi:10.1140/epjst/e2015-02603-8.
[35] Savi MA. Nonlinear dynamics and chaos in shape memory alloy systems. International Journal of Non-Linear Mechanics 2015;70. doi:10.1016/j.ijnonlinmec.2014.06.001.
[36] Li DZ, Feng ZC. Dynamic properties of pseudoelastic shape memory alloys. Smart Mater Struct 1997. doi:10.1117/12.275696.
[37] Doare O, Sbarra A, Touzé C, Moussa MO, Moumni Z. Experimental analysis of the quasi-static and dynamic torsional behaviour of shape memory alloys. International Journal of Solidsand Structures 2012. doi:10.1016/j.ijsolstr.2011.09.009.
[38] de Aguiar RAA, Savi MA, Pacheco PMCL. Experimental investigation of vibration reduction using shape memory alloys. J Intell Mater SystStruct 2013;24.
[39] Enemark S, Savi MA, Santos IF. Nonlinear dynamics of a pseudoelastic shape memory alloy system-theory and experiment. Smart Mater Struct 2014;23. doi:10.1088/0964-1726/23/8/085018.
[40] Enemark S, Santos IF, Savi MA. Modelling, characterisation and uncertainties of stabilised pseudoelastic shape memory alloy helical springs. Intell Mater Syst Struct 2016;27. doi:10.1177/1045389X16635845.
[41] Saadat S, Salichs J, Noori M, Hou Z, Davoodi H, Bar-on I, et al. An overview of vibration and seismic applications of NiTi shape memory alloy. Smart Mater Struct 2002. doi:10.1088/0964-1726/11/2/305.
[42] Wang W, Fang C, Liu J. Large size superelastic SMA bars: heat treatment strategy, mechanical property and seismic application. Smart Mater Struct 2016. doi:10.1088/0964-1726/25/7/075001.
[43] Varela S, Saiddi M. A bridge column with superelastic NiTi SMA and replaceable rubber hinge for earthquake damage mitigation. Smart Mater Struct 2016. doi:10.1088/0964-1726/25/7/075012.
[44] deSouza CV, deMarqui C. Experimental study on the aeroelastic behavior of a typical airfoil section with superelastic shape memory alloy springs. J Intell Mater SystStruct 2018;29. doi:10.1177/1045389X17721024.
[45] deSouza CV, deMarqui C. Adaptive locally resonant metamaterials leveraging shape memory alloys. Journal of Applied Physics 2018;124 doi:10.1063/1.5031168.
[46] dosReis RPB, Silva PCS, Senko R, Silva AA, deAraujo CJ. Methodology for the estimation of material damping as applied to superelastic shape memory alloy mini-springs. Materials and Design 2019;161. doi:10.1016/j.matdes.2018.11.012.
[47] Vignoli LL, Savi MA, El-Borgi S. Nonlinear dynamics of earthquake-resistant structures using shape memory alloy composites. J Intell Mater SystStruct 2020;31(5). doi:10.1177/1045389X19898269.
[48] Eggeler G, Hornbogen E, Yawny A, Heckmann A, Wagner M. Structural and functional fatigue of NiTi shape memory alloys. Materials Science and Engineering: A 2004;378(1):24–33. doi:10.1016/j.msea.2003.10.327.
[49] Zhang Y, You Y, Anlas G, Zhu J, Zhang W. Experimental and theoretical investigation of the frequency effect on low cycle fatigue of shape memory alloys. International Journal of Plasticity 2017;90. doi:10.1016/j.ijplas.2016.11.012.
[50] Dornelas VM, deOliveira SA, Savi MA. A macroscopic description of shape memory alloy functional fatigue. International Journal of Mechanical Sciences 2020;170:105345. doi:10.1016/j.ijmecsci.2019.105345.
[51] Wang D, Fotinich Y, Carman GP. Influence of temperature on the electromechanical and fatigue behavior of piezoelectric ceramics. J Appl Phys 1998;83(10):5342–50. doi:10.1063/1.367362.
[52] Peddigari M, Kim GY, Park CH, Min Y, Kim JW, Ahn CW, Choi JJ, Hahn BD, Choi JH, Park DS, Hong JK, Yeom JT, Park KI, Jeong DY, Yoon WH, Ryu J, Hwang GT. A comparison study of fatigue behavior of hard and soft piezoelectric single crystal macro-fiber composites for vibration energy harvesting. Sensors 2019;19(9):2196. doi:10.3390/s19092196.
[53] Salazar R, Serrano M, Abdelkefi A. Fatigue in piezoelectric ceramic vibrational energy harvesting: a review. Applied Energy 2020;270:115161. doi:10.1016/j.apenergy.2020.115161.
[54] Fan Z, Koruza J, Rödel J, Tan X. An ideal amplitude window against electric fatigue in BaTio3-based lead-free piezoelectric materials. Acta Materialia 2018;151:253–9. doi:10.1016/j.actamat.2018.03.067.
[55] Savi MA, Pacheco PMCL, Garcia MS, Aguiar LFG, Souza RAA, daHora RB. Nonlinear geometric influence on the mechanical behavior of shape memory alloy helical springs. Smart Mater Struct 2015;24. doi:10.1088/0964-1726/24/3/035012.
[56] Leo DJ. Engineering analysis of smart materials and structures. John Wiley and Sons, Inc; 2007.
[57] Erturk A, Inman DJ. Issues in mathematical modeling of piezoelectric energy harvesters. Smart Mater Struct 2008;17(6). doi:10.1088/0964-1726/17/6/065016.